Review

SEMICONDUCTOR MATERIALS FOR ULTRAFAST OPTOELECTRONIC APPLICATIONS

A. Krotkus [a], K. Bertulis [a], R. Adomavičius [a], V. Pačebutas [a], and A. Geižutis [a,b]

[a] *Semiconductor Physics Institute, A. Goštauto 11, LT-01108 Vilnius, Lithuania*
E-mail: andrejus@opel2.pfi.lt

[b] *Department of Electronic Systems, Vilnius Gediminas Technical University, Naugarduko 41, LT-03227 Vilnius, Lithuania*

The paper presents a review of experimental investigations of various semiconductor materials used for the development of ultrafast optoelectronic devices activated by femtosecond laser pulses that have been performed at the Optoelectronics Laboratory of the Semiconductor Physics Institute during the period from 1997 to 2008. Technology and physical characteristics of low-temperature-grown GaAs and GaBiAs layers as well as the effect of terahertz radiation from the femtosecond laser excited semiconductor surfaces are described and analysed.

Keywords: THz time domain spectroscopy, low temperature grown GaAs, low temperature grown GaBiAs, photoconductor antenna

PACS: 78.47.+p, 73.50.Pz, 73.40.Sx, 71.55.Eq

1. Introduction

Terahertz (THz) frequency range that is spanning from several hundreds of GHz to approximately 10 THz is lately attracting an enhanced interest due to its applications in spectroscopy, imaging, and sensing of various, mainly organic and biological, substances. The number of such applications is steadily increasing as new advanced techniques for electromagnetic radiation generation and detection in this frequency range are appearing. One of such techniques that has largely contributed to the progress in the field of THz technology is the so-called THz time-domain-spectroscopy (TDS), which uses short pulses of broadband THz radiation generated using femtosecond laser pulses, a technique that has evolved from the research performed in 1980s [1, 2]. Although spectral resolution of THz-TDS is rather coarse, worse than that of narrow-band spectroscopic techniques such as Fourier transform spectroscopy, it has several important advantages. Because TDS systems measure THz electric field rather than its power, this measurement is more sensitive and contains time-resolved phase information. Moreover, a good THz beam quality of those systems allows their implementation in various imaging applications providing rich spectral information.

Femtosecond laser pulses are converted to short pulses of electromagnetic radiation, whose spectral content could be several tens of THz by using components made of semiconducting or nonlinear optic materials. Similar components are then used for measuring the temporal shape of THz pulses. The main advantage of the semiconductors is that photoconductive components manufactured from these materials are more efficient THz emitters and more sensitive THz detectors, thus they can be used even with low power diode or fibre lasers. However, semiconductor materials, which these components are made of, should meet a set of quite unique requirements: they should have very short, sub-picosecond carrier lifetimes accompanied by moderate electron mobility, a rather rare combination of materials' parameters. Most widely known of such materials is so-called low-temperature-grown GaAs (LTG GaAs).

This article describes the work in investigating semiconductor materials used for THz photonics applications performed during the last decade at the Optoelectronics laboratory of the Semiconductor Physics Institute in Vilnius, Lithuania. It consists of three main parts. Firstly, we will describe the research on LTG GaAs and other GaAs crystals with large deviations from crystal stoichiometry that is the main cause of their unusual physical properties. Later on, technology and physical properties of novel semiconductor material, LTG GaBiAs, that could be used in THz-TDS systems activated by long-wavelength lasers will be presented.

The last part of the article is devoted to a group of physical effects leading to an interesting phenomenon, THz pulse generation at the semiconductor surfaces illuminated by femtosecond laser pulses.

2. Nonstoichiometric GaAs

2.1. Growth and structural characterization of Be-doped LTG GaAs

Since the discovery of unique semi-insulating and ultrafast carrier recombination properties of low-temperature molecular-beam-epitaxy (MBE) grown GaAs [3], it has become the most important material for applications in ultrafast optoelectronics [4, 5]. Short carrier lifetimes and high resistivity in this material have been shown to result from excess arsenic in the form of arsenic antisite As_{Ga} and gallium vacancy V_{Ga} point defects [6]. Ionized As_{Ga} defects, the density of which is approximately three times larger than that of V_{Ga} [7], serve as the main electron traps. Because the V_{Ga} density is much lower than the concentration of As_{Ga} defects, only a few percent of As-antisites are ionized and can participate in the electron trapping, while the rest of antisites remain inactive. Therefore, attempts have been made to activate neutral As_{Ga} centres by additionally doping LTG GaAs with compensating acceptor impurities. A natural choice of the acceptor species in GaAs is beryllium, which is known for being readily incorporated during the MBE growth.

Epitaxial LTG GaAs layers were grown on semi-insulating (100)-oriented GaAs substrates in a solid source molecular-beam-epitaxy (MBE) system. As_4/Ga beam equivalent pressure rate equal to 10 and a growth rate of 1.5 μm/h were used for all growth runs. The substrates were bonded to a molybdenum holder using high purity indium solder. After common cleaning of substrate surface from oxides, 500 nm thick GaAs buffer layer was grown at 600 °C substrate temperature, then the growth was interrupted and the temperature was lowered to 280 °C (as measured by a thermocouple fixed at the substrate holder). Beryllium doping was performed in the range of its nominal concentrations (N_{Be}) from $5 \cdot 10^{17}$ to $2 \cdot 10^{19}$ cm^{-3}. The thickness of LTG GaAs:Be layers was ranging from 1 to 3 μm. Three differently Be-doped layers were isochronally annealed in a MBE reactor under arsenic ambient for 20 min at temperatures ranging from 500 to 800 °C.

The structure of the LTG GaAs layers was studied by cross-sectional transmission electron microscopy (XTEM) on several as-grown and annealed samples [8].
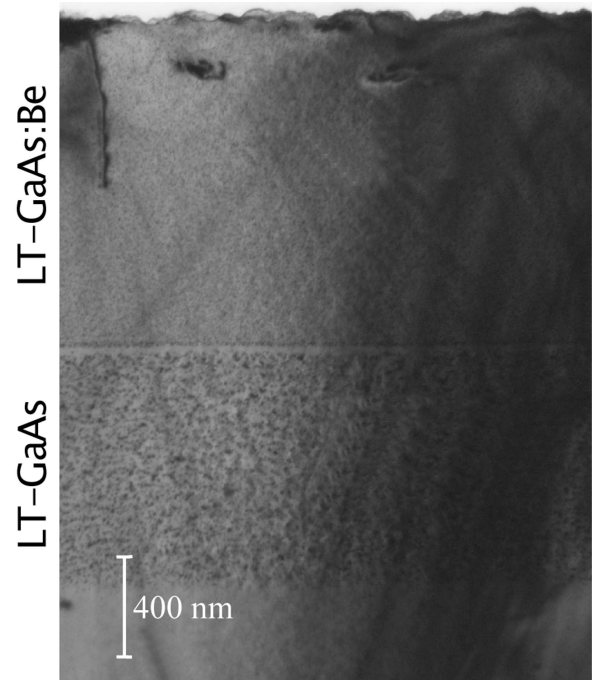

Fig. 1. XTEM image of a specially grown layered epitaxial structure (corresponding to Ref. [8]).

As-grown layers with $N_{Be} = 1.5 \cdot 10^{18}$ cm^{-3} were of high crystalline quality up to a thickness of about 3 μm. The effect of beryllium doping on the precipitate formation is illustrated in Fig. 1, where an XTEM image of a grown layered epitaxial structure is presented. This structure, annealed at 600 °C, consisted of a 0.5 μm thick GaAs buffer layer covered by an undoped 1.2 μm thick LTG GaAs layer, and then by a 1.7 μm thick Be-doped ($N_{Be} = 3.5 \cdot 10^{18}$ cm^{-3}) LTG GaAs layer. Both LTG GaAs layers are mostly discernible because of a high density of As precipitates (almost invisible on this picture for the top layer) that are formed during the annealing. Beryllium doping leads to a decrease of the average As precipitate diameter, which is in agreement with the previous results [9]. High crystalline quality of the Be-doped material is also clearly seen in Fig. 1.

The structure of Be-doped LTG GaAs layers was also studied by the X-ray quasi-forbidden reflection (XQFR) method [10] and by high-resolution X-ray diffraction technique (XRD) [11]. The first of these methods employs, for example, (002) and (006) reflections in the GaAs structure. They are called quasi-forbidden because of very small differences in scattering factors between gallium and arsenic and are very sensitive to the chemical composition of the crystal. It has been shown in [10] that in as-grown LTG GaAs:Be the beryllium dopant substitutes for Ga atoms and introduces some local lattice distortions. These conclusions were confirmed by the results of XRD experiments [11]. Fig-
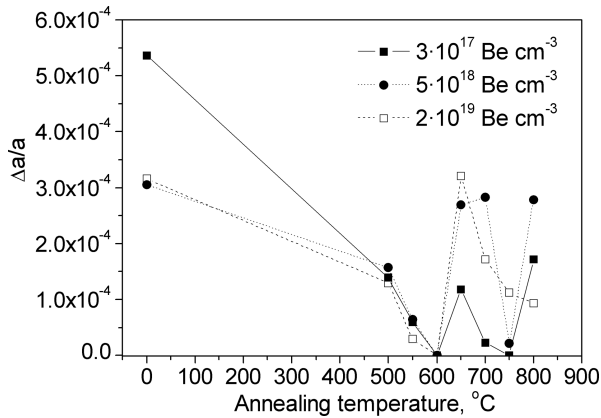
Fig. 2. Relative lattice parameter mismatch between the LTG GaAs:Be layer and the substrate as a function of the annealing temperature (corresponding to Ref. [15]).
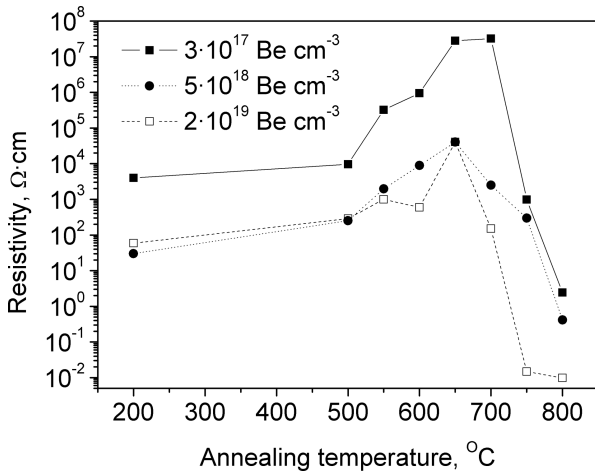

Fig. 3. Resistivity of the LTG GaAs layer as a function of the annealing temperature (corresponding to Ref. [15]).

ure 2 presents the relative lattice parameter mismatch between the LTG GaAs:Be layer and substrate as a function of annealing temperature. Increasing the annealing temperature to 600 °C results in a complete relaxation of crystalline lattice of the layer and all lattice parameter differences vanish. At that temperature the full width at half maximum of the rocking curve is the smallest for all three Be concentrations used in the experiments. At larger annealing temperatures, the lattice mismatch appears again, most probably, due to the increase of Be impurity mobility and their activation as acceptors [12]. Because Be atoms in LTG GaAs layers are substitutional, they prevent vacancy assisted diffusion of As into precipitates and stabilize As_{Ga} defects.

Measurements of electrical transport characteristics have shown that resistivity of the samples generally increases after annealing and reaches maximum at the annealing temperatures of about 650 °C (see Fig. 3 [8]). Annealing reduces the number of As_{Ga}, leading to a
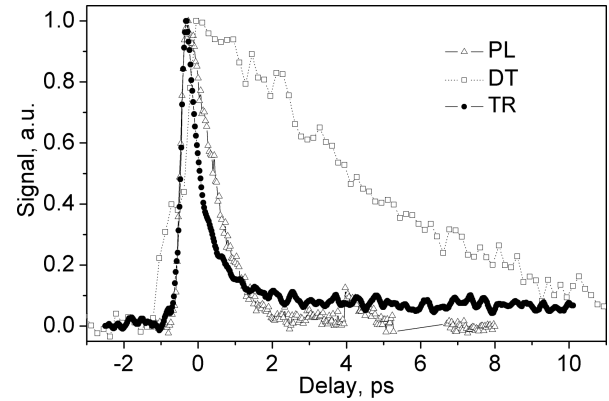

Fig. 4. Photogenerated carriers' dynamics measured by three different techniques on LTG GaAs layer grown at 250 °C and annealed at 650 °C. PL is temporally-resolved photoluminescence up-conversion, DR is dynamic optical reflectivity, and DT is two-colour dynamic transmitivity (corresponding to Refs. [8, 13]).

decrease of the hopping conductivy that is dominating electrical transport in as-grown LTG GaAs samples. For annealing temperatures above 700 °C, a decrease in resistivity is observed. It is probably due to a more efficient activation of Be acceptors, which leads also to the appearance of p-type conduction.

Summarizing the results presented in this section, doping of LTG GaAs with beryllium enhances the materials' homogeneity by preventing the nucleation of the As-precipitates. Layers with the highest resistivity that are most appropriate for manufacturing THz radiation components can be obtained when Be doping is rather moderate ($N_{Be} \sim (3–4) \cdot 10^{17}$ cm^{-3}) and over a very limited range of the annealing temperatures of about 650 °C.

2.2. Carrier dynamics in LTG GaAs

Dynamical properties of photoexcited nonequilibrium electrons were studied by several techniques, which include time-resolved photoluminescence up-conversion (PL), dynamic optical reflectivity (DR), dynamic photoconductivity (PC), and two-colour dynamic transmitivity (DT). In the first three experiments 100 fs duration pulses from a Ti:sapphire laser with a central wavelength of $\sim$800 nm were used. In the case of DT, 800 nm pulses were used for carrier excitation, whereas 1450 nm wavelength pulses were used for probing the dynamics of electron trap population.

Figure 4 illustrates transients measured by three different techniques on LTG GaAs layer grown at 250 °C and annealed at 650 °C [8, 13]. The characteristic decay time of the PL and TR transients as well as the rise time of DT transient are of the order of 500 fs and are interpreted as the electron capture time. On the other hand,
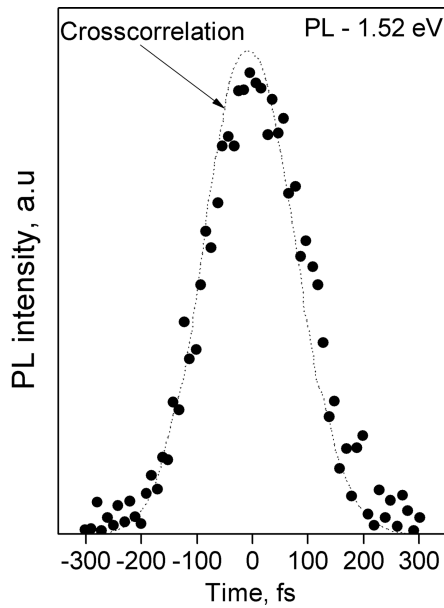
Fig. 5. PL transient in arsenic ion implanted GaAs annealed at 500 OC. A cross-correlation between the pump and probe laser pulses is shown by a full curve (corresponding to Ref. [14]).

Fig. 6. PL spectra in (a) annealed and (b) as-grown LTG GaAs. Points are the experimental data measured at the peaks of PL transients, full curve inicates the results of a Monte Carlo molecular dynamics simulation for carrier trapping times of (a) 30 fs and (b) 70 fs (corresponding to Ref. [14]).

the decay of DT signal is characterized by a time constant of the order of several picoseconds that is defined by the trap emptying rate.

In as-grown LTG GaAs layers, the electrons are trapped on a time scale shorter than 100 fs, therefore this dynamics is impossible to investigate by using standard pump-and-probe techniques. In [14] we studied electron trapping in as-grown LTG GaAs indirectly, by investigating PL spectral dependences. Because photoexcited electrons in this material are captured by the trapping centres faster than they reach thermal distribution, the photoluminescence spectrum is peaking not at the vicinity of the band-edge energy (∼1.4 eV for GaAs) but around the photoexcitation energy. Figure 5 shows a typical PL transient at a photon energy of 1.52 eV as measured by up-conversion technique in as-grown LTG GaAs. As can be seen, PL curve is nearly the same as the cross-correlation between the pump pulse and the light scattered from the sample surface. This means that the electrons are present in the sample only during the light pulse and their lifetime is shorter that the laser pulse duration of 100 fs. The PL spectrum measured at the peaks of the transients is shown in Fig. 6; it monotonously decreases on the both sides of a maximum situated near the energy at which the electrons are excited by the laser pulse. Comparison of this spectrum with the one measured under the same conditions on an annealed LTG GaAs allows a rough estimation of carrier lifetimes by interpolating the missing parts of the spectrum and assuming the same
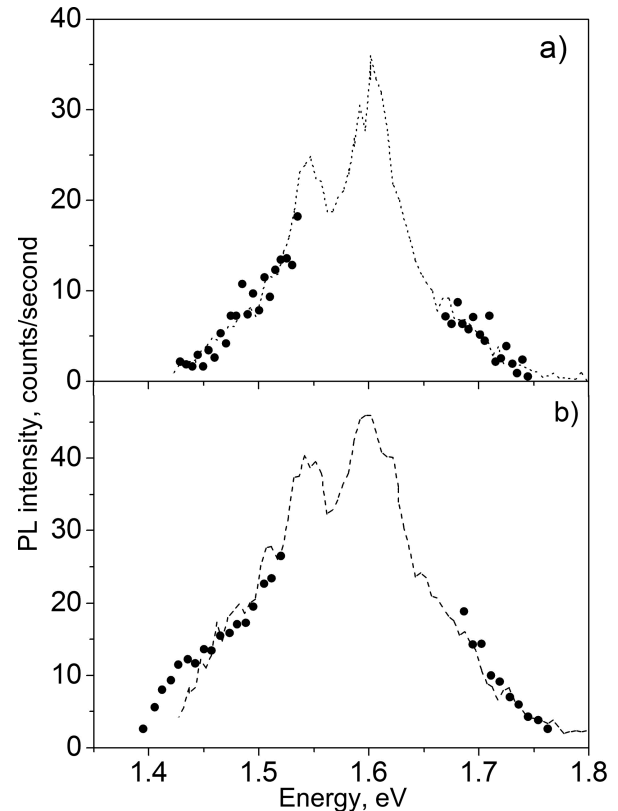
probability of radiative transitions in both as-grown and annealed samples, we obtain a value of 60 fs for carrier lifetime in as-grown LTG GaAs. A slightly larger value of this lifetime (70 fs) was obtained by comparing the measured PL spectrum with the results of the numerical simulation using Monte Carlo / molecular dynamic technique [14]. Comparing carrier lifetimes in as-grown and annealed LTG GaAs has been very important for resolving the debate on which one of the competing models – As-precipitate model [15] or deep As antisite trap model [16] – is adequately describing electron recombination in this material, in favour of the second one.

Electron trapping times in Be doped LTG GaAs was determined in [17]. It has been found that, contrary to the expectations, these times are growing with the increase of the Be-acceptor density. An abrupt reduction of the electron trapping time is observed only in annealed LTG GaAs at rather high doping levels. This behaviour can be explained if we assume that at least some of the Be atoms occupy the sites of gallium vacancies in the lattice. In non-doped LTG GaAs V_{Ga} are the
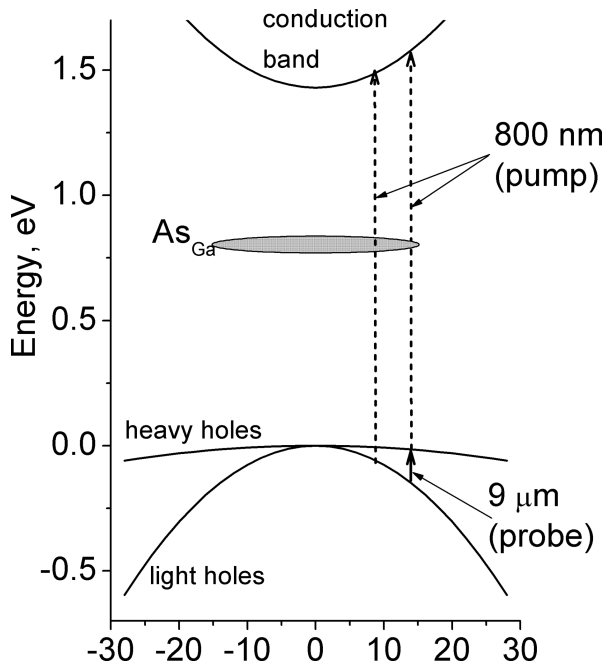
Fig. 7. Energy band structure of LTG GaAs (corresponding to Ref. [19]).

main acceptors that compensate deep As_{Ga} donors and determine the density of ionized As_{Ga}^+ electron traps. Because V_{Ga} is a triple acceptor [18], its replacement by Be, which is a single-ionized acceptor, would lead to the reduction of As_{Ga}^+ as long as N_{Be} is less than the density of V_{Ga}.

The information on hole trapping processes in LTG GaAs is scarce, although it is as essential as the electron trapping parameters for the design of devices working at high repetition frequencies. Direct monitoring of the photoexcited hole density dynamics in the valence band of LTG GaAs was performed by using two-colour pump-and-probe technique [19]. Nonequilibrium carriers were excited by femtosecond near-infrared (800 nm) pulses and probed with 9 μm wavelength mid-infrared pulses. The latter wavelength corresponds to the transitions between the heavy and light hole valence bands (Fig. 7), these transitions being approximately by one order of magnitude more intense than the free-electron absorption. It has been found in [19] that the hole trapping time in as-grown LTG GaAs is of the order of 1 ps and more that 10 times longer in the annealed material. The correlation of the values of this parameter with the changes of As_{Ga} defect state induced by additional doping of the layers has led to the conclusion that photoexcited holes in LTG GaAs are mainly trapped by neutral As antisites.

Since the main defects determining photoexcited carrier trapping in LTG GaAs are ionized and neutral As antisites, the most important parameters describing this process are the density of those antisites and their capture cross-sections for electrons and holes. These parameters, which are determining electron and hole trapping times via relation

$$\frac{1}{\tau_{n,p}} = \sigma_{n,p} N_{n,p} \nu_{n,p}, \tag{1}$$

were evaluated in [8]. In formula (1) τ_n and τ_p are the electron and hole trapping times, σ_n and σ_p are their capture cross-sections, N_n and N_p are their densities, and ν_n and ν_p are their thermal velocities, respectively. Electron and hole trapping cross-sections have been found to be of the order of $\sigma_n = 10^{-13}$ and $\sigma_p = 10^{-15}$ cm^2, respectively.

2.3. Ion-implanted GaAs

An alternative to low-temperature MBE growth way of producing highly non-stoichiometric GaAs is the implantation of this crystal by large doses of high energy As ions [20, 21]. Ion implantation has the advantage of incorporating controlled amounts of excess arsenic and also the flexibility of creating the non-stoichiometry in localized regions of a wafer. As-implanted and subsequently annealed GaAs has been found to have electrical and recombination characteristics close to those of LTG GaAs [21]. For example, electron trapping time in GaAs implanted by 2 MeV energy As ions was equal to 30 fs before annealing [14] and 1 ps after annealing at 600 °C temperature [21], respectively.

Surprisingly, similar results were obtained also after implanting GaAs by other heavy ions: Ga [22], Si, and O [23]. Trapping time dependences on the implantation dose for four implanted species after 600 °C annealing are shown in Fig. 8. A monotonic decrease of the trapping times with increasing implantation dose is observed in all cases. The values of the carrier trapping times in GaAs implanted at a certain dose of different ions are surprisingly close to each other, although some correlation with the atomic mass of the implanted element is observable: shorter trapping times are present in materials irradiated by heavier ions. Later investigations [24, 25] have shown that the mechanism of ultrafast carrier recombination in ion-implanted GaAs is essentially the same as in LTG GaAs, i. e. their capture to the non-stoichiometry related point defects. A comparison of these two non-stoichiometric GaAs materials from the point of view of their application in THz optoelectronic devices has been made in [26]. It is shown in Fig. 9, where electron and hole trapping times in GaAs obtained by different technology are presented.
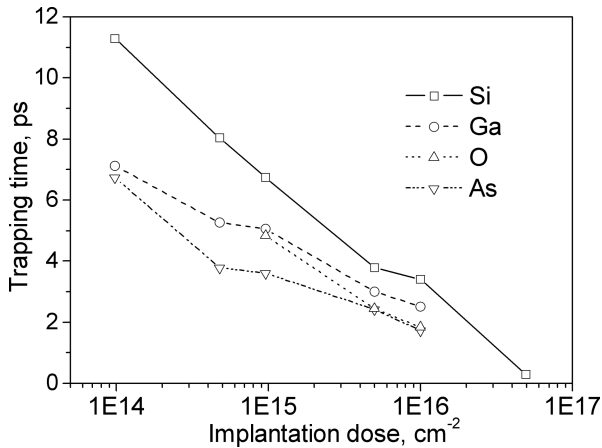
Fig. 8. Measured trapping time in implanted GaAs as a function of the dose of four different implants. Ion energy was 2 MeV (As, Ga, and O) and 1 eV (Si); all samples were annealed at 600 °C after implantation (corresponding to Refs. [22, 23]).
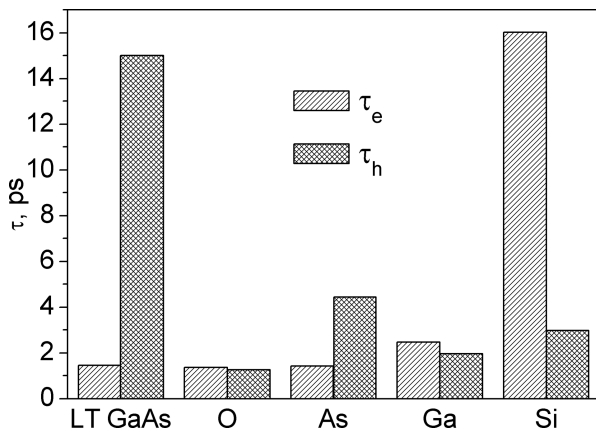

Fig. 9. Electron and hole lifetimes in different non-stoichiometric GaAs materials (corresponding to Ref. [26]).

Laser activated THz emitters and detectors are, essentially, photoconductive components integrated with wide-band antennae, therefore, Si-implanted GaAs can be excluded from the consideration because of its large electrical conductivity and rather long electron trapping times. On the other hand, As, Ga, and O-implanted GaAs are highly resistive after thermal annealing and can be used as substrates for THz photoconductors. Electron trapping times in these crystals are quite short; however, they approach 1 ps only when the implantation dose is very large ($\geq 10^{16}$ cm^{-2}). For such large doses, electron mobility in the material becomes small, thus a wide bandwidth of the device is achievable only at the cost of its lower efficiency and sensitivity. From this point of view the use of LTG GaAs is more preferable, because the electron mobility in this material remains at a satisfactory level even when their trapping times are much shorter than 1 ps. However, ion-implanted GaAs crystals are, in general, character-

ized by considerably shorter hole trapping times than LTG GaAs. Short hole trapping times are essential for such devices as cw THz emitters and detectors based on the optical mixing effects [27].

3. GaBiAs layers for THz optoelectronic applications

3.1. GaBiAs technology and material properties

The majority of the optoelectronic THz systems are presently using femtosecond Ti:sapphire lasers emitting at the wavelengths around 800 nm and photoconductive components made of LTG GaAs epitaxial layers. Because the Ti:sapphire laser requires a rather complicated, many-stage optical pumping arrangement, these systems are quite bulky and complicated. One solution to this problem would be using lasers emitting in the spectral ranges close to 1 or 1.5 μm, which can be directly pumped by laser diode bars. However, the absorption edge of GaAs is at the wavelengths of $\sim$0.9 μm, thus this material is not suitable for devices activated by compact, diode-pumped solid-state or fibre lasers emitting at longer wavelengths. These wavelengths could be employed in InGaAs, however, attempts to grow LTG InGaAs have led to only limited success because the shortest carrier lifetimes achieved are only $\sim$2 ps [28], and, most importantly, the material has low resistivity, which is a serious obstacle for its applications in photoconductors. InGaAs layers with subpicosecond lifetimes and reasonably high resistance were obtained only by the implantation with MeV energy ions [29, 30], which is a unique and costly procedure.

Our choice for material for THz optoelectronic devices activated by long-wavelength laser pulses was GaBiAs alloy. Previously, there have been several attempts to grow GaBiAs on GaAs substrates by MBE technique. The main purpose of these efforts was to produce a material with weaker, compared to other III–V compounds, temperature dependence of bandgap energy for the applications in diode laser active layers [31, 32]. It has been found [33] that the bandgap of GaBiAs decreases with the increase of Bi content much faster than for adding In in InGaAs, consequently, the lattice mismatch between GaBiAs alloy and GaAs substrate is up to four times smaller compared to InGaAs with the corresponding bandgap.

Because Bi is a large atom as compared to both Ga and As, it has a tendency of a surface segregation and is difficult to incorporate into the crystalline lattice under
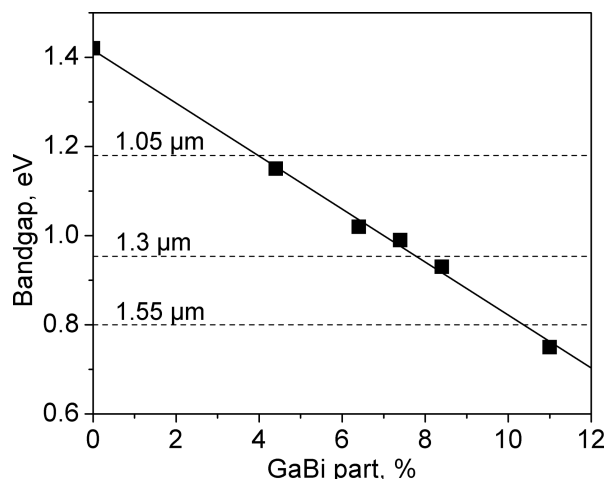
Fig. 10. Energy bandgap of $GaBi_xAs_{1-x}$ as a function of the Bi content in the layer (corresponding to Ref. [35]).

standard MBE growth conditions. Therefore, in order to obtain a significant Bi incorporation it is necessary to perform the growth at surface temperatures much lower than ~600 °C that are typical of MBE growth of GaAs [33]. Reduced growth temperature could, as in the case of LTG GaAs, lead to the presence of structural defects acting as fast traps for non-equilibrium current carriers, which would impair the performance of light emitters made of GaBiAs layers but could be advantageous for ultrafast photoconductive devices manufactured on their basis [34].

GaBiAs layers were grown on semi-insulating GaAs substrates with 3° off crystallographic (100) planes in a solid-state MBE system. After a standard substrate cleaning from oxides, a GaAs buffer layer of 500 nm thickness was grown at 600 °C with As/Ga beam equivalent pressure ratio (BEPR) of about 20. Then the growth was interrupted and the substrate temperature was lowered down to temperatures in the range from 240 to 330 °C (lower than the growth temperatures from 350 to 410 °C used in [32]) with simultaneous decreasing of BEPR to about 7 in order to grow a 400 nm thick LTG GaAs and, immediately afterwards, a GaBiAs layer. Finally, an 8–15 μm thick protective GaAs cap layer was grown on top of the structure at the same temperature as was used for GaBiAs growth.

Bismuth content in epitaxial layers was measured by two techniques: XRD using a Cu $K\alpha_1$ line and Rutherford backscattering spectroscopy [35]; both techniques have led to very close results for all GaBiAs layers investigated. Energy bandgap of the $GaBi_xAs_{1-x}$ alloys was also investigated by several independent experiments: spectral measurements of optical absorption, photoconductivity, and photoluminescence. The results of different experiments are summarized in

Fig. 10, where the bandgap of $GaBi_xAs_{1-x}$ is shown as a function of Bi content in the layer. As can be seen in this figure, the rate of the bandgap reduction with increasing Bi content is approximately equal to -62 meV/%Bi, which coincides with the data obtained previously [36] and is much larger than a corresponding parameter for $In_xGa_{1-x}As$ alloy (-12 meV/%In) [37].

Electrical parameters of the layers were investigated by the Hall-effect and resistivity measurements. Conductivity of all layers was of p-type, with a hole concentration of the order of 10^{14} to 10^{15} cm^{-3} and the resistivity in some of the cases was larger than 2000 Ω cm. The electron mobility in $GaBi_xAs_{1-x}$ layers was determined from the optical pump – THz probe experiments [38, 39]. It has been found to be as large as 2000 cm^2/(V s) [38] and 2800 cm^2/(V s) [39], much larger than electron mobility in LTG GaAs.

It has been shown in [40] that large bandgap shift of $GaBi_xAs_{1-x}$ can be explained by a valence band anti-crossing model as the result of the interaction between the extended states in GaAs valence band and resonant T2 states of the Bi atoms. Comparing with GaNAs alloy, where similar bandgap shift is caused by a conduction band anti-crossing [41], low-temperature-grown GaBiAs is more suitable for photoconductive applications. Nitrogen creates resonant donor levels in GaNAs causing the reduction of the dark resistivity of the layers, whereas acceptor levels introduced by Bi in GaBiAs can enhance the compensation of As_{Ga} donors created during the growth of this alloy at low temperatures and increase both the dark resistivity and the electron trapping rate. Moreover, the lowest conduction subband in GaNAs is characterized by a very low electron mobility [42], in contrast with GaBiAs, where the conduction band states do not mix with the impurity states and the effect of the latter on the electron mobility is minimal.

3.2. Optoelectronic THz radiation components from GaBiAs

Photoexcited carrier relaxation in GaBiAs layers has been studied by the optical pump – THz probe technique. Yb:KGW laser pulses (wavelength of 1030 nm, pulse duration of 70 fs, and pulse repetition rate of 76 MHz); THz radiation pulses were emitted and detected using a photoconductive antennae made of LTG GaBiAs. A 1.8 mm diameter pinhole was used to overlap THz and visible beams on the sample. The spot size of the optical pump beam was larger than the diameter of the pinhole so that the THz probe pulses have
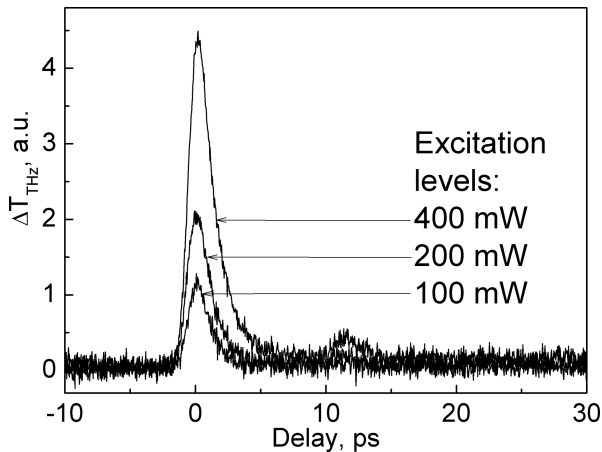
Fig. 11. Optically induced THz absorption transients measured on a GaBi$_{0.08}$As$_{0.92}$ sample grown at 260 °C for three different excitation levels (corresponding to Ref. [62]).
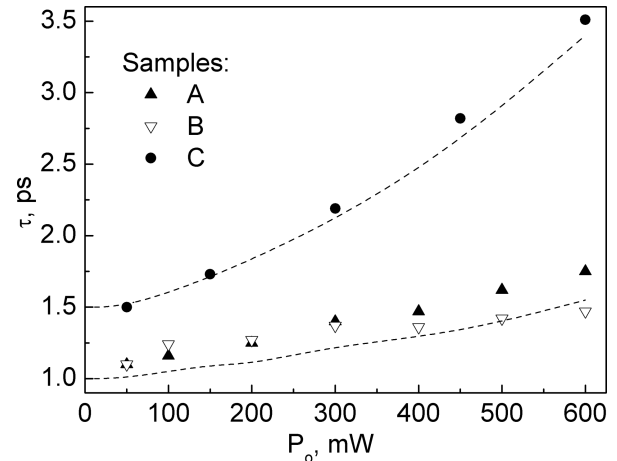

Fig. 12. Excitation level dependences of the apparent electron lifetimes for three GaBi$_x$As$_{1-x}$ samples. Points are experiment, curves are modelling (corresponding to Ref. [62]).

been sampling nearly uniformly photoexcited sample region. The temporal resolution of this measurement was ∼800 fs; carrier lifetimes were studied when the average power of the optical pump beam was changed from 50 to 600 mW, which is corresponding to photoexcited electron and hole densities in the range from 10^{15} to $2 \cdot 10^{16}$ cm^{-3}. These measurements were performed at room temperature.

Figure 11 presents the results of this pump-and-probe experiment performed on a GaBi$_{0.08}$As$_{0.92}$ sample grown at 260 °C for three different photoexcitation levels. Two main features are evident on these experimental traces. Firstly, the dynamics of the optically induced THz absorption that is represented by the curves shown on Fig. 11 clearly consists of two parts: a faster decaying initial part that is, most probably, caused by trapping of more mobile electrons and a much slower decaying tail which can be attributed to hole trapping. Secondly, the characteristic time of the fast decaying part of the dynamics is increasing with the intensity of the pump beam, a feature that is usually associated with trap filling and saturation effects.

The latter effect can be used for estimating electron trap characteristics of the material by comparing experimental values of the apparent electron density decay times at various excitation intensities with a corresponding theoretical dependence. If one assumes that the holes are trapped much slower than the electrons, the latter dependence can be found by solving the rate equations for free and trapped electrons n and n_t, respectively:

$$\frac{\mathrm{d}n}{\mathrm{d}t} = G(t) - \sigma_\mathrm{t} n (N_\mathrm{t} - n_\mathrm{t}) \nu_\mathrm{th}, \qquad (2)$$

$$\frac{\mathrm{d}n}{\mathrm{d}t} = \sigma_\mathrm{t} n (N_\mathrm{t} - n_\mathrm{t}) \nu_\mathrm{th}. \qquad (3)$$

Here $G(t)$ is the photocarrier generation rate by a Gaussian shaped femtosecond laser pulse, σ_t is the electron trapping cross-section, N_t is the trap density, and ν_th is the thermal velocity of the electrons.

Figure 12 presents the experimental values of the electron decay time as a function of average pump beam intensity for three different LTG GaBiAs layers with their best fit to the results of the modelling. This fitting has yielded the following values of the electron trap parameters in LTG GaBiAs: $\sigma_\mathrm{t} = 4 \cdot 10^{-13}$ cm^2, $N_\mathrm{t} = 2.8 \cdot 10^{16}$ cm^{-3} (for the layer *A*) and $N_\mathrm{t} = 4.2 \cdot 10^{16}$ cm^{-3} (for the layers *B* and *C*). Comparing these values with the corresponding As$_\mathrm{Ga}$ trap parameters in LTG GaAs with similar electron trapping times, one can see that the electron capture cross-section in LTG GaBiAs is approximately 4 times larger [8]. This can be understood when one remembers that GaBiAs is p-type material, therefore As$_\mathrm{Ga}$ donors in this material can be double-ionized, thus their attractive potential can be stronger and capture cross-section larger than for single-ionized donors. Because As$_\mathrm{Ga}$ donors are fully ionized, short electron lifetimes in GaBiAs are achieved at much lower overall As$_\mathrm{Ga}$ densities than in LTG GaAs where only a small part of these defects are ionized and act as electron capture centres. This makes LTG GaBiAs prospective material for pulsed optoelectronic THz radiation emitters and detectors.

Photoconductive THz detectors manufactured from LTG GaBiAs layers were, for the first time, demonstrated in [43]. By using 70 fs duration pulses from a Yb:KGW laser and a p-InAs crystal as a surface emitter, the spectral width of more than 2 THz and the signal-
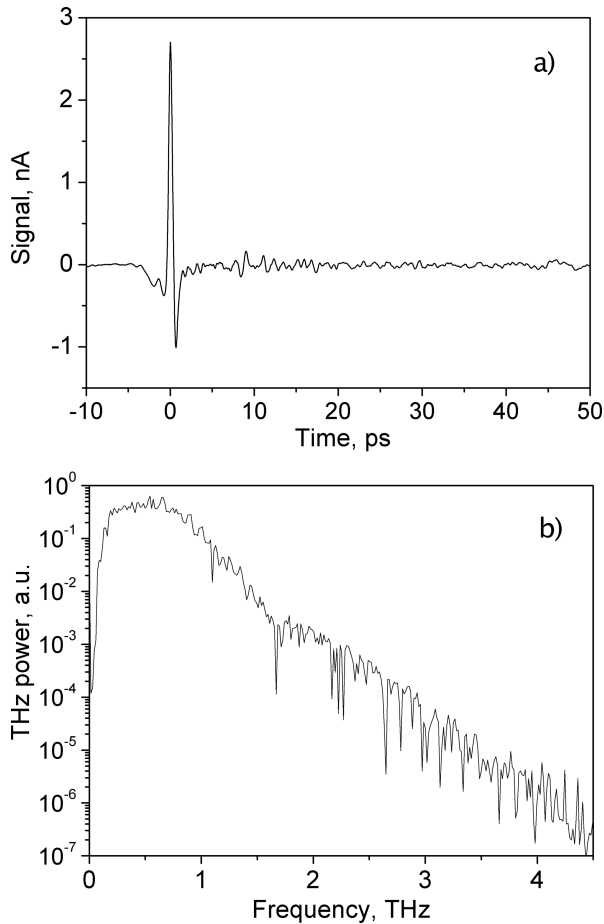
Fig. 13. (a) Shape of the THz pulse and (b) its Fourier spectrum. The emitter and detector are made of GaBiAs (corresponding to Ref. [43]).

to-noise power ratio of 60 dB were reached. Even better parameters have been achieved when LTG GaBiAs photoconductors were used both for THz pulse generation and its detection [44]. In this case, in order to achieve larger dark resistances of the emitters, mesa-etching of the bismide-arsenide layer was used leaving only the active part of the GaBiAs layer in the photoexcited gap region. Figure 13 shows the shape of the obtained THz pulse and its Fourier spectrum. As seen from this figure, the frequency spectrum of the THz transient extends as far as to ∼4.5 THz; at the high frequency side it is, most probably, limited by the absorption in the GaAs substrate.

4. Semiconductor surface emitters

4.1. Mechanisms of the surface emission

The majority of semiconductor crystals when illuminated with femtosecond laser pulses radiate THz radiation pulses. Generally speaking, THz radiation at the photoexcited semiconductor surface can be emitted by a dipole that is induced either due to a fast changing photocurrent or by the nonlinear polarization of the material. In the far field region, the THz field can be expressed as

$$E_{\mathrm{THz}} = -\frac{S}{c^2 R} \int\limits_0^\infty \left(\frac{\partial j}{\partial t} + \frac{\partial^2 P}{\partial t^2} \right) \mathrm{d}z \,, \qquad (4)$$

where c is the speed of light in vacuum, R is the distance from the point of observation to the emitting region, S is the area of the laser excited spot on the semiconductor surface; j and P are the photocurrent and nonlinear polarization components in the direction of the THz wave polarization, respectively. Integration in the relation (4) is carried out over the depth z. It is important to point out that the expression (4) is correct when the diameter of the illuminated spot is smaller than the wavelength of the emitted THz radiation, otherwise the dipole approach is not correct and THz field amplitude should be determined by summing up the partial waves emitted by the separate surface elements and by taking into account their phase relations. In following we will discuss different physical mechanisms leading to the appearance of the transient photocurrent or low-frequency nonlinear polarization components entering relation (4).

Electrons and holes that are optically generated in a semiconductor due to the absorption of femtosecond laser radiation are spatially separated by the built-in or external electric field, which results in a transient photocurrent varying on a subpicosecond time scale. This fast varying photocurrent can be an effective source of THz radiation with the amplitude defined by the time derivative of the photocurrent. This mechanism of THz generation is known as a photocurrent surge effect and it is realized in THz emitters made of the semiconductors with a strong band bending at their surface.

In the so-called photo-Dember effect a spatial separation of electrons and holes occurs due to their different mobilities. Photoexcited electrons diffusing from their excitation point at the surface towards the bulk of the material surpass the less mobile holes and, as a result, the space charge and the electric field appear. This electric field starts to slow down the photoelectrons and to accelerate the holes, therefore, eventually both types of photocarriers start to move as a single quasineutral packet. The photo-Dember effect has been usually studied for the case of a stationary photoexcitation when the drift-diffusion approach is correct. In this case, the Dember photovoltage is typically low, of the order of 10^{-2} V. However, in the majority III–V

and IV–VI narrow-gap materials the characteristic time of the electron–LO phonon scattering is around 200 fs; these scattering processes lead only to small changes in electron momentum, therefore, during the first few hundreds of femtoseconds after the photoexcitation excitation, the electron motion is purely ballistic rather than diffusive. As the result, the Dember photovoltages in these materials can be quite large, of the order of 1 V and more.

The lowest order nonlinear optical response of a non-centrosymmetric crystal is caused by the second order susceptibility χ_2 that leads to the sum and difference frequency generation. In the case when the optical beam contains nearly the same frequencies (which is typical of femtosecond laser spectra) and interacts nonlinearly with the crystal, the difference frequency is in the dc range and the induced polarization is referred as optical rectification (OR) with the induced charge displacement following the optical pulse envelope. When a built-in dc field E_s is present at the semiconductor surface, transient THz polarization can also be induced due to the third-order nonlinear susceptibility χ_3; the THz pulse magnitude generated due to this electrical-field-induced optical rectification (EFIOR) effect will be proportional to the effective second order susceptibility $\chi_2 \chi_2^{\text{eff}} = \chi_3 E_s$.

As a fingerprint of nonlinear optical THz pulse generation mechanisms, the dependence of the emitted THz pulse amplitude on the orientation of the optical field with regard to the crystallographic axes is usually considered. It has to be pointed out that these so-called azimuthal angle dependences of the THz emission efficiency from zinc-blende semiconductors like GaAs measured at different crystallographic planes can also help in distinguishing between OR and EFIOR mechanisms [45, 46].

When considering THz emission from the surfaces of particular semiconductor materials, simultaneous action of several physical mechanisms, both of the photocurrent surge type and nonlinear optical effects, should be taken into account. Figure 14 presents a comparison of THz pulse amplitudes emitted under the same experimental conditions from the surfaces of several semiconductor materials at two femtosecond laser wavelengths: 800 nm, corresponding to the Ti:sapphire laser and 1.03 μm (Yb:KGW laser). In the following we will discuss the main features of this effect in some materials in detail.
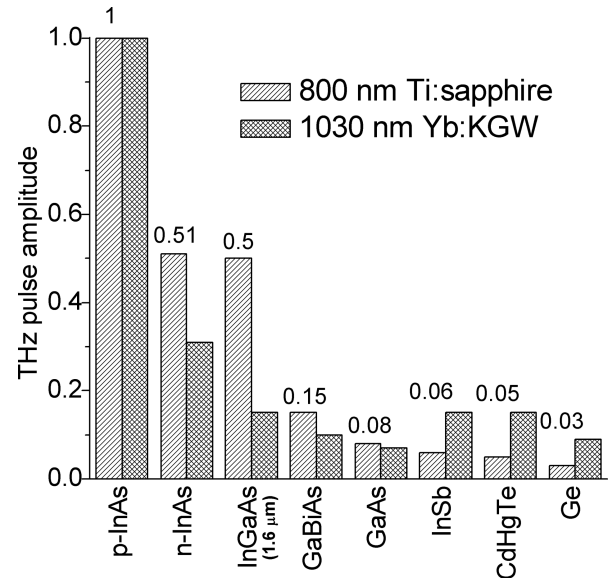

Fig. 14. Comparison of THz emission efficiency from various semiconductors' surfaces excited by a femtosecond laser at 1030 and 800 nm wavelengths (corresponding to Ref. [63]).

4.2. Indium arsenide

Most efficiently THz radiation is generated from the surfaces of InAs crystal, especially when a strong magnetic field is applied in parallel to those surfaces [47]. This magnetic field influence had focused the attention of researchers on the photo-Dember effect, although some authors also pointed out a possible role of other phenomena such as bulk optical rectification [48], magneto-plasma waves [49], or coupled plasmon–phonon modes [50] in THz radiation from InAs surface. Possible influences of the surface electric field were usually written off due to a narrow band gap in InAs and potentially small band bending at the surface of this material. This is not always justifiable, because surface potential in InAs is fixed at fairly high (0.2 eV [51]) energies above the conduction band edge and in p-doped crystal the surface depletion layer can be sufficiently wide and strong. It has been discovered in [52] that p-type InAs is a better THz emitter than n-type InAs, and this was explained by a contribution of the EFIOR effect. Later on, analysis of the symmetry of the azimuthal angle dependences of THz radiation, performed in [45] by illuminating different crystal planes of n-InAs, has pointed out to the predominance of the EFIOR effect also in n-doped crystals, although the origin of surface electric field necessary for the occurrence of this effect remained unclear.

On the other hand, dependences of the THz radiation efficiency from femtosecond laser illuminated InAs surfaces on photon energy measured in [53] are leading to
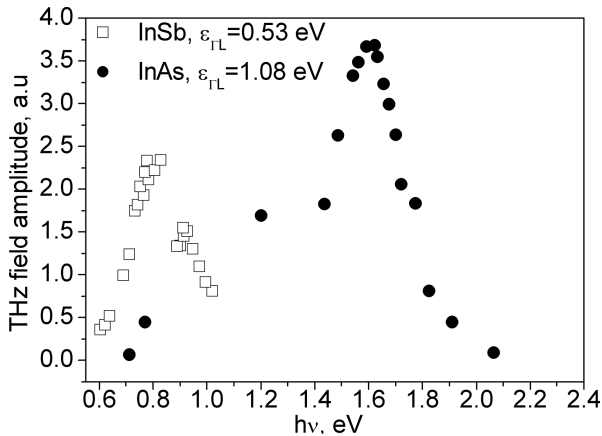
Fig. 15. Dependence of the THz radiation efficiency from InAs surface illuminated by femtosecond laser with different photon energy (corresponding to Ref. [53]).

an opposite conclusion. The results of such measurements are presented in Fig. 15. THz field amplitude increases with increasing photon energy, reaches its maximum at $h\nu = 1.6$ eV, and then decreases. Such a shape of the spectral dependence for THz emission could be explained if one assumes that the free carrier contribution due to the photo-Dember effect is dominating. When photon energies are large enough, the electrons are excited high in the conduction band, where they are efficiently scattered to subsidiary L and X valleys of the conduction band with large effective masses. Intense inter-valley scattering impedes electron and hole spatial separation and leads to the reduction of photo-Dember voltage.

This seeming contradiction was resolved in [54] by proposing the mechanism of THz generation in InAs that takes into account both the photo-Dember and EFIOR effect contributions. It has been proposed [54] that surface electric field necessary for the appearance of the effective second-order optical nonlinearity and the EFIOR effect is nucleated by the excited electron and hole separation. The electric field created by photocarriers excited at the leading part of the laser pulse is rectifying the rest of the laser pulse and that way is leading to the THz generation. The validity of this model has been confirmed by the experiments employing double-pulse excitation of the sample and by Monte Carlo simulation [54].

4.3. Other semiconductors

Figure 14 compares THz pulse amplitudes radiated at the surfaces of various semiconductors after their illumination by femtosecond pulses of two different wavelength lasers under the same conditions. As seen

from the diagram presented on this figure, the closest to InAs are the parameters of THz emitters made of In-GaAs alloy with a rather wide energy band gap, whereas such narrow-gap semiconductors as InSb or CdHgTe are poor THz emitters. This evidences that small band gap and large excess energy of photoexcited electrons are not the most important factors determining efficient THz pulse generation. On the opposite, electrons with large excess energies will be additionally scattered to the subsidiary valleys as in InSb [53] or their effective mass will significantly increase (CdHgTe [55]), thus the electron separation from the holes will be less efficient and the Dember photovoltage induced by this separation will be relatively small.

When analysing physical mechanisms responsible for THz emission from different materials it is interesting to note that in many cases several phenomena are taking place in a single semiconductor. For GaAs excited with a laser quanta smaller that its band gap ε_g, THz emission is caused by the optical rectification effect [56]; when photon energy is comparable to ε_g, the current surge effect starts to dominate in THz pulse emission [57]. It also has to be pointed out that nonlinear optical effects play an important role in THz generation from the majority of semiconductor surfaces. The azimuthal angle dependences of THz radiation measured on (112) surface of InSb have evidenced that in this material both second-order (optical rectification) and third-order (EFIOR effect) contributions are of a comparable order of magnitude [58]. In centrosymmetrical Ge crystals, for which the second-order nonlinear optical susceptibility is zero, THz radiation is caused by a combined action of the EFIOR effect and the photo-Dember current surge [59].

A great variety of physical phenomena leading to the THz pulse generation from the semiconductor surfaces provides unique possibilities for studying various parameters of these materials. Investigations of THz radiation from femtosecond laser excited semiconductor surfaces were already used for determining the inter-valley energy separation in the conduction bands of various compounds [53], the electron inter-valley scattering rate in Ge [60], and the electron energy relaxation rate in CdHgTe [61].

5. Conclusion

The intense development of THz-TDS systems has led to the discovery of a new group of semiconductor materials that are characterized by shorter than 1 ps carrier recombination times and relatively high electron

mobility that are of a critical importance for the design of THz radiation detectors activated by femtosecond laser pulses. This unique combination of the material properties realized, e. g., in LTG GaAs or LTG GaBiAs epitaxial layers has its origin in the presence of non-stoichiometry related As-antisite defects. As-antisite defects have exceptionally large electron capture cross-section, therefore, they are causing ultrafast carrier recombination even at moderate defect densities that do not significantly affect the electron mobility. Sensitive, wide-band detectors activated by 800 nm laser pulses are manufactured from LTG GaAs and LTG GaBiAs layers and can be used for making similar detectors activated by 1 μm and longer wavelength laser pulses.

Carrier lifetime is not limiting the use of semiconductors in another application important for THz-TDS systems, the development of THz pulse emitters. When excited by femtosecond laser pulses the majority of these materials radiate THz pulses from their surfaces. Stronger or weaker THz pulses are emitted from practically all weakly or moderately doped semiconductors. Besides a universal occurrence of this effect, emission from semiconductor surfaces provides wider and better shaped THz beams than those generated by photoconductive antennae, which could be preferable for some specific applications like THz imaging. Several different physical phenomena can lead to this effect. The best THz emitter is p-type InAs; this is due to a simultaneous action of the photo-Dember voltage induced by the photoexcited electron and hole separation and the electrical-field induced optical rectification effect.

Acknowledgements

References

[1] D.H. Auston, K.P. Cheung, J.A. Valdmanis, and D.A. Kleinan, Phys. Rev. Lett. **53**, 1555 (1984).

[2] Ch. Fattinger and D. Grischkowsky, Appl. Phys. Lett. **53**, 1480 (1988).

[3] F.W. Smith, A.R. Calawa, C.L. Chen, M.J. Manfra, and L.J. Mahoney, IEEE Electron Dev. Lett. **9**, 77 (1988).

[4] J.F. Whitaker, Mater. Sci. Eng. **B22**, 61 (1993).

[5] D.D. Nolte, J. Appl. Phys. **85**, 6259 (1999).

[6] Z. Liliental-Weber, H.J. Cheng, S. Gupta, J. Whitaker, K. Nichols, and W. Smith, J. Electron. Mater. **22**, 1465 (1993).

[7] M. Lyusberg, H. Sohn, A. Prasad, P. Specht, Z. Liliental-Weber, E.R. Weber, J. Gebauer, and R. Krause-Rehberg, J. Appl. Phys. **83**, 561 (1998).

[8] A. Krotkus, K. Bertulis, M. Kaminska, K. Korona, A. Wolos, J. Siegert, S. Marcinkevičius, J.-F. Roux, and J.-L. Coutaz, IEE Proc., Optoelectron. **149**, 111 (2002).

[9] M.R. Melloch, N. Otsuka, K. Mahalingam, C. Chang, J.M. Woodall, G.D. Pettit, P.D. Kirchner, F. Cardone, A.C. Warren, and D.D. Nolte, J. Appl. Phys. **72**, 3509 (1992).

[10] I. Frymark, G. Kowalski, M. Kaminska, and A. Krotkus, J. Alloys Compounds **362**, 261 (2004).

[11] G. Kowalski, I. Frymark, A. Krotkus, K. Bertulis, and M. Kaminska, Mater. Sci. Eng. **B91-92**, 449 (2002).

[12] D.E. Bliss, W. Walukiewicz, J.W. Ager, E.E. Haller, K.T. Chan, and S. Tanigawa, J. Appl. Phys. **71**, 1699 (1992).

[13] H. Eusebe, J.F. Roux, J.-L. Coutaz, and A. Krotkus, J. Appl. Phys. **98**, 033711 (2005).

[14] S. Marcinkevičius, A. Krotkus, R. Viselga, U. Olin, and C. Jagadish, Semicond. Sci. Technol. **12**, 398 (1997).

[15] A.C. Warren, J.M. Woodall, J.F. Freeouf, D. Grischkowsky, D.T. McInturf, M.R. Melloch, and N. Otsuka, Appl. Phys. Lett. **57**, 1331 (1990).

[16] M. Kaminska and E.R. Weber, *The Physics of Semiconductors*, eds. E.M. Anastasskis and J.D. Joannopoulos (World Scientific, Singapore, 1990) p. 473.

[17] A. Krotkus, K. Bertulis, L. Dapkus, U. Olin, and S. Marcinkevičius, Appl. Phys. Lett. **75**, 3336 (1999).

[18] S.B. Zhang and J.E. Nothrup, Phys. Rev. Lett. **67**, 2339 (1991).

[19] R. Adomavičius, A. Krotkus, K. Bertulis, V. Sirutkaitis, R. Butkus, and A. Piskarskas, Appl. Phys. Lett. **83**, 5304 (2003).

[20] A. Claverie, F. Namavar, and Z. Liliental-Weber, Appl. Phys. Lett. **62**, 1271 (1993).

[21] A. Krotkus, S. Marcinkevičius, J. Jasinski, M. Kaminska, H.H. Tan, and C. Jagadish, Appl. Phys. Lett. **66**, 3304 (1995).

[22] C. Jagadish, H.H. Tan, J. Jasinski, M. Kaminska, M. Palczewska, A. Krotkus, and S. Marcinkevičius, Appl. Phys. Lett. **67**, 1724 (1995).

[23] C. Jagadish, H.H. Tan, A. Krotkus, S. Marcinkevičius, K. Korona, and M. Kaminska, Appl. Phys. Lett. **68**, 2225 (1996).

[24] L. Giniūnas, R. Danielius, H.H. Tan, C. Jagadish, R. Adomavičius, and A. Krotkus, Appl. Phys. Lett. **78**, 1667 (2001).

[25] S. Marcinkevičius, C. Jagadish, H.H. Tan, M. Kaminska, K. Korona, R. Adomavičius, and A. Krotkus, Appl. Phys. Lett. **76**, 1308 (2000).

[26] A. Geižutis, R. Adomavičius, A. Urbanowicz, K. Bertulis, A. Krotkus, H.H. Tan, and C. Jagadish, Lithuanian J. Phys. **48**, 249 (2005).

[27] E.R. Brown, K.A. Macintosh, K.B. Nichols, and C.L. Denis, Appl. Phys. Lett. **66**, 285 (1995).

[28] J.M. Kim, Y.T. Lee, J.D. Song, and J.H. Kim, J. Cryst. Growth **265**, 8 (2004).

[29] C. Carmody, H.H. Tan, C. Jagadish, A. Gaarder, and S. Marcinkevičius, Appl. Phys. Lett. **82**, 3912 (2003).

[30] N. Chimot, J. Manegeney, L. Joulaod, P. Crozat, H. Bernas, K. Blary, and J.F. Lampin, Appl. Phys. Lett. **87**, 193510 (2005).

[31] M. Yoshimoto, S. Murata, A. Chayahara, Y. Horino, J. Saraie, and K. Oe, Jpn. J. Appl. Phys., Part 2, **42**, L1235 (2003).

[32] S. Tixier, M. Adamcyk, T. Tiedje, S. Francoeur, A. Mascarenhas, P. Wei, and P. Schietekatte, Appl. Phys. Lett. **82**, 2245 (2003).

[33] S. Francoeur, M.J. Seong, A. Mascarenhas, S. Tixier, M. Adamcyk, and T. Tiedje, Appl. Phys. Lett. **82**, 3874 (2003).

[34] K. Bertulis, A. Krotkus, G. Aleksejenko, V. Pačebutas, R. Adomavičius, G. Molis, and S. Marcinkevičius, Appl. Phys. Lett. **88**, 20113 (2006).

[35] V. Pačebutas, K. Bertulis, L. Dapkus, G. Aleksejenko, A. Krotkus, K.M. Yu, and W. Walukiewicz, Semicond. Sci. Technol. **22**, 818 (2007).

[36] M. Yoshimoto, W. Huang, G. Feng, and K. Oe, Phys. Status Solidi B **7**, 1421 (2006).

[37] I. Vurgaftman, J.R. Meyer, and I.R. Ram-Mohan, J. Appl. Phys. **89**, 5815 (2001).

[38] V. Pačebutas, K. Bertulis, G. Aleksejenko, and A. Krotkus, J. Mater. Sci. Mater. Electron. **20**, S363 (2009).

[39] D.G. Cook, F.A. Hegmann, E.C. Young, and T. Tiedje, Appl. Phys. Lett. **89**, 122103 (2006).

[40] K. Alberi, O.D. Dubon, W. Walukiewicz, K.M. Yu, K. Bertulis, and A. Krotkus, Appl. Phys. Lett. **91**, 051909 (2007).

[41] Y. Zhang, A. Mascarenhas, and L.W. Wang, Phys. Rev. B **71**, 155201 (2006).

[42] W. Shan, K.M. Yu, W. Walukiewicz, J. Wu, J.W. Ager, and E.E. Haller, J. Phys. Cond. Matter **16**, S3355 (2004).

[43] G. Molis, R. Adomavičius, A. Krotkus, K. Bertulis, L. Giniūnas, J. Pocius, and R. Danielius, Electron. Lett. **43**, 190 (2007).

[44] V. Pačebutas, A. Bičiūnas, K. Bertulis, and A. Krotkus, Electron. Lett. **44**, 1154 (2008).

[45] M. Reid, I.V. Cravetchi, and R. Fedosejevs, Phys. Rev. B **72**, 035201 (2005).

[46] V.L. Malevich, A. Krotkus, A. Bičiūnas, and V. Pačebutas, J. Appl. Phys. **104**, 113117 (2008).

[47] N. Sarukura, H. Ohtake, S. Izumida, and Z. Liu, J. Appl. Phys. **84**, 654 (1998).

[48] P. Gu, M. Tani, S. Kono, K. Sakai, and X.-C. Zhang, J. Appl. Phys. **91**, 5533 (2002).

[49] J.N. Heyman, P. Neocleous, D. Hebert, P.A. Crowell, T. Müller, and K. Unterrainer, Phys. Rev. B **64**, 085202 (2001).

[50] M.P. Hasselbeck, D. Stalnaker, L.A. Schlie, T.J. Rotter, A. Stintz, and M. Sheik-Bahae, Phys. Rev. B **65**, 233203 (2002).

[51] C. Affentaugschegel and H.H. Wieder, Semicond. Sci. Technol. **16**, 708 (2001).

[52] R. Adomavičius, A. Urbanowicz, G. Molis, and A. Krotkus, Appl. Phys. Lett. **85**, 2463 (2004).

[53] R. Adomavičius, G. Molis, A. Krotkus, and V. Sirutkaitis, Appl. Phys. Lett. **87**, 261101 (2005).

[54] A. Krotkus, R. Adomavičius, G. Molis, and V.L. Malevich, J. Nanolectron. Optoelectron. **2**, 108 (2007).

[55] A. Krotkus, R. Adomavičius, G. Molis, A. Urbanowicz, and H. Eusebe, J. Appl. Phys. **96**, 4006 (2004).

[56] X.-C. Zhang, Y. Jin, K. Yang, and L.J. Schowalter, Phys. Rev. Lett. **69**, 2303 (1992).

[57] G. Molis, A. Krotkus, and V. Vaičaitis, Appl. Phys. Lett. **94**, 091104 (2009).

[58] V.L. Malevich, A. Krotkus, A. Bičiūnas, and V. Pačebutas, J. Appl. Phys. **104**, 113117 (2008).

[59] A. Urbanowicz, A. Krotkus, R. Adomavičius, and V.L. Malevich, Physica B **398**, 98 (2007).

[60] A. Urbanowicz, R. Adomavičius, A. Krotkus, and V.L. Malevich, Semicond. Sci. Technol. **20**, 1010 (2005).

[61] R. Adomavičius, R. Šustavičiūtė, and A. Krotkus, in: *Proceedings of the 13th International Conference on Narrow-Gap Semiconductors 2007*, Guilford, England, p. 41.

[62] V. Pačebutas, K. Bertulis, A. Bičiūnas, and A. Krotkus, Phys. Status Solidi C [accepted].

[63] A. Bičiūnas, V. Pačebutas, and A. Krotkus, Physica B **404**, 3386 (2009).

PUSLAIDININKINĖS MEDŽIAGOS ULTRASPARČIAJAI OPTOELEKTRONIKAI

A. Krotkus [a], K. Bertulis [a], R. Adomavičius [a], V. Pačebutas [a], A. Geižutis [a,b]

[a] *Puslaidininkių fizikos institutas, Vilnius, Lietuva*
[b] *Vilniaus Gedimino technikos universitetas, Vilnius, Lietuva*

Santrauka

Pateikta įvairių puslaidininkinių medžiagų, naudojamų kuriant ultrasparčius optoelektronikos prietaisus, žadinamus femtosekundiniais lazeriais, eksperimentinių tyrimų apžvalga. Tyrimai atlikti Puslaidininkių fizikos instituto Optoelektronikos laboratorijoje 1997–2008 metais. Aprašyta žemoje temperatūroje augintų GaAs ir GaBiAs sluoksnių technologija ir fizikinės savybės. Išsamiai aptartas ir išanalizuotas THz spinduliuotės generavimas iš femtosekundiniu lazeriu sužadintų puslaidininkių paviršiaus.